SIMULATION OF IMPACT DAMAGE IN LAMINATED COMPOSITES BY PROGRESSIVE DAMAGE MODELS

Dianshi Feng*, Agostino Cerioni, Francesco Aymerich

Department of Mechanical, Chemical and Materials Engineering
University of Cagliari, Piazza d'Armi, 09123 Cagliari, Italy

**dianshi@iris.unica.it*

Keywords: Laminate, Low-velocity impact, 3D failure model, Finite element modelling.

Abstract
The paper describes the development of a finite element (FE) tool for prediction of initiation, growth and interaction of the different damage mechanisms developing in composite structures subjected to low-velocity impact. The numerical results obtained by FE models are compared with experimental observations from instrumented impact tests carried out at various impact energies. Good agreement is observed between numerical predictions and experimental results in terms of contact force history, peak force value, absorbed energy and projected damage area.

1 Introduction

Laminated composite materials are being increasingly used in load bearing structures for many engineering fields, including aerospace, automotive, marine and wind turbine applications, because of their high strength and stiffness to weight ratios, good fatigue performance and excellent corrosion resistance. However, the application of composite laminates in primary structures is still limited by the difficulty in predicting their service life. Composite laminates are extremely susceptible to internal damage caused by foreign object impact events, which can be reasonably expected during the whole life of a structure including manufacturing, service and maintenance [1]. Damage induced by impact consists of a combination of various intralaminar (matrix cracks and fibre fracture) and interlaminar (delaminations) failure modes, which, even if undetectable by visual inspection, may severely degrade mechanical properties of the material and lead to final collapse of the structure.

Various impact test procedures and destructive or non-destructive inspection techniques are available to characterize damage induced by impact in composite laminates. Experimental tests are however extremely time-consuming and cost-intensive, because of the large variety of possible structural configurations and loading conditions. Furthermore, physical phenomena involved in impact events are very complex, thus restricting the applicability of analytical models to the investigation of simple geometries and loading cases. For this reason, appropriate material models and reliable numerical procedures are greatly needed to understand and predict the damage response of composite structures under impact.

Various models and criteria have been proposed in the last decades to describe and simulate damage initiation and progressive degradation of composite materials subjected to low-velocity impacts. Continuum damage mechanics (CDM), originally proposed by Kachanov [2] and further developed by Lemaitre and Chaboche [3], has been increasingly used in recent

years to simulate impact damage phenomena in composite laminates. Iannucci et al. [4] developed and implemented a two-dimensional CDM model into the explicit FE package LS-DYNA to predict matrix cracks and fibre fracture in composite laminates subjected to elevated strain rates. The model was later improved and extended to a full 3D formulation [5,6]. Donadon et al. [5] developed a 3D failure model that includes shear non-linearities and shear damage using a coupled semi-empirical elasto-damageable-plastic material law. Analogous damage models were recently used in [7] to simulate the response of a stiffened composite panel under low-velocity impact.
In this study, a fully three-dimensional failure model was developed and used to predict initiation, growth and interaction of the different damage mechanisms developing in composite laminates subjected to low-velocity impact. Damage and fracture mechanisms typically observed in impacted laminate plates (delaminations between layers with different fibre orientation, fibre fracture and matrix cracking) were simulated and implemented in the FE package ABAQUS/Explicit through a specialized user-defined subroutine (Vumat). The numerical results are illustrated and compared with experimental observations from instrumented impact tests carried out at various impact energies.

2 Experimental tests

The impact response of $[0_3/+45/-45]_s$ laminates was examined in this study. Laminates were made of HS300/ET223 graphite/epoxy prepreg plies (supplied by Seal) with a fibre weight ratio of 0.65. Rectangular specimens 65 mm × 87.5 mm in size and with a nominal thickness of 3.2 mm were prepared for impact testing.
An instrumented drop-weight testing machine was used to apply low-velocity impacts by a 2.34 kg impactor with a hemispherically ended rod of 12.5 mm in diameter. The force–time history and the impactor velocity just before the impact, as respectively measured by a strain-gauge bridge bonded to the impactor tup and by an infra-red sensor, were recorded by a data acquisition unit. The absorbed energy and the history of indentor displacement were calculated by numerical integrations of the force–time trace. During impact testing, the laminate panels were simply supported on a steel plate with a 45 mm × 67.5 mm rectangular opening. The panels were impacted with energies ranging between approximately 1 J and 8 J, obtained by varying the drop height of the impactor. Finally, internal damage in impacted panels was assessed by penetrant-enhanced X-radiography.
A series of tests were also carried out on coupon samples to characterize elastic, strength and fracture properties to be used in the FE model for simulation of the impact phenomenon.

3 Failure model

3.1 Intralaminar failure

The intralaminar damage models implemented in this study follow the approach illustrated and discussed in [5,8,9] and are based on these assumptions: 1) the damage process is smeared over the finite element dimension; 2) internal damage variables (d_{ij}) are introduced to quantify damage extent and stiffness degradation associated to specific fibre or matrix damage modes; 3) stress/strain based initiation criteria and fracture energy based evolution laws are defined for each specific failure mode.
Each of the internal damage variables (d_{ij}) will affect different components of the fictitious undamaged stress tensor $\bar{\sigma}$ (effective stress tensor), which can be related to the true stress tensor σ through damage matrix D as:

$$\sigma = D\bar{\sigma} = DE\varepsilon \tag{1}$$

where, E denotes the undamaged material stiffness matrix [10]. Based on the hypotheses of strain equivalence [3] and on elastic-plastic strain decomposition, the following explicit incremental material relationship can be obtained:

$$\Delta\sigma = E[D\{\Delta\varepsilon - \Delta\varepsilon^{in}\} - \Delta D\{\varepsilon - \varepsilon^{in}\}] \tag{2}$$

where $\Delta\sigma$ is the stress incremental vector; the strain incremental vector $\Delta\varepsilon$ can be decomposed into elastic $\Delta\varepsilon^{el}$ and inelastic parts $\Delta\varepsilon^{in}$; D and ΔD are defined as damage and incremental damage matrices respectively [5].

3.1.1 Fibre failure modes

Two similar failure criteria were used to detect fibre tensile and compressive damage initiation:

$$\begin{aligned} F_{11}^{t}(\varepsilon_{11}) &= \left(\frac{\varepsilon_{11}}{\varepsilon_{11}^{0t}}\right)^2 - 1 \geq 0 \\ F_{11}^{c}(\varepsilon_{11}) &= \left(\frac{\varepsilon_{11}}{\varepsilon_{11}^{0c}}\right)^2 - 1 \geq 0 \end{aligned} \tag{3}$$

A coupled tension-compression damage evolution law was adopted by imposing the following equations:

$$d_{11} = d_{11}^{c} + d_{11}^{t} - d_{11}^{c} d_{11}^{t} \tag{4}$$

with,

$$\begin{aligned} d_{11}^{t}(\varepsilon_{11}) &= \frac{\varepsilon_{11}^{ft}(\varepsilon_{11} - \varepsilon_{11}^{0t})}{\varepsilon_{11}(\varepsilon_{11}^{ft} - \varepsilon_{11}^{0t})} \\ d_{11}^{c}(\varepsilon_{11}) &= \frac{\varepsilon_{11}^{fc}(\varepsilon_{11} - \varepsilon_{11}^{0c})}{\varepsilon_{11}(\varepsilon_{11}^{fc} - \varepsilon_{11}^{0c})} \end{aligned} \tag{5}$$

In order to model matrix crushing and fragment interaction effects within the crushing zone, the longitudinal direct stress of buckled fibres is degraded to a minimum residual stress, which is assumed equal to the matrix compressive stress as shown in Fig. 1.

3.1.2 Matrix tensile failure

Damage initiation and evolution for tensile matrix cracking were defined using the following failure criteria:

$$\begin{aligned} F_{22}^{t}(\varepsilon_{22}) &= \left(\frac{\varepsilon_{22}}{\varepsilon_{22}^{0t}}\right)^2 - 1 \geq 0 \\ d_{22}^{t}(\varepsilon_{22}) &= \frac{\varepsilon_{22}^{ft}(\varepsilon_{22} - \varepsilon_{22}^{0t})}{\varepsilon_{22}(\varepsilon_{22}^{ft} - \varepsilon_{22}^{0t})} \end{aligned} \tag{6}$$

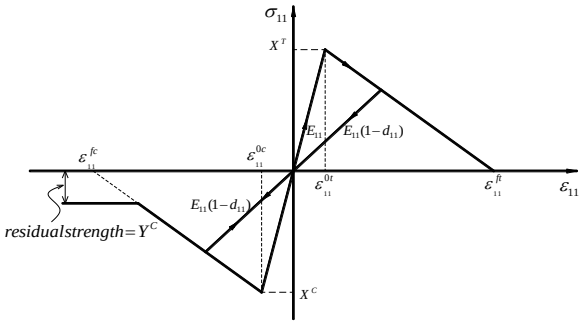

Figure 1. Damage model behaviour for fibre failure

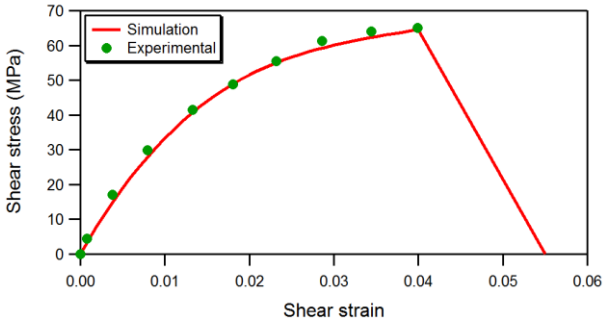

Figure 2. Test results on nonlinear shear failure mode

3.1.3 Matrix compressive failure

The damage model for simulating transverse failure under compression follows the Mohr failure theory originally proposed by Hashin [11] and then further extended by Puck and Shurmann [12]. Details about this approach may be found in [5,7].

3.1.4 Nonlinear shear failure modes

Experimental evidence indicates that composite materials show a nonlinear and irreversible behavior under shear loading. As an example, Fig. 2 shows a typical shear stress-strain relation as obtained by tests on [+45/-45]s laminates of the same prepreg material used for impacted plates. The nonlinear response may be attributed to two distinct mechanical processes [7]: plasticity and stiffness reduction due to progressive damage. The total shear strain can thus be decomposed into elastic and damage strain:

$$\gamma_{ij} = \gamma_{ij}^{e} + \gamma_{ij}^{d} \qquad i, j = 1,2,3 \qquad i \neq j \tag{7}$$

To represent the nonlinear shear behavior, a cubic polynomial stress-strain curve was introduced:

$$\tau_{ij}(\gamma_{ij}) = c_1\gamma_{ij} + c_2\gamma_{ij}^2 + c_3\gamma_{ij}^3 \tag{8}$$

where c_1 , c_2 and c_3 are coefficients determined by fitting the polynomial expression to the experimentally obtained shear stress-shear strain curve.

The proposed shear failure model is characterized by two distinct phases (see Fig. 2). The first phase corresponds to the nonlinearly increasing stage up to the maximum shear stress; in this region, the damage parameter is defined as:

$$d_{ij}(\gamma_{ij}) = \alpha\gamma_{ij} \qquad \gamma_{ij} \leq \gamma_{ij}^{\max} \tag{9}$$

where α is a material constant, determined experimentally by cyclic loading-unloading tests, which expresses the gradual shear modulus reduction with increasing strain. The second phase is represented by a linear softening law, described by the following equation:

$$d_{ij}(\gamma_{ij}) = \alpha\gamma_{ij}^{\max} + \frac{\gamma_{ij}^{f}(\gamma_{ij} - \gamma_{ij}^{\max})}{\gamma_{ij}(\gamma_{ij}^{f} - \gamma_{ij}^{\max})} - \alpha\gamma_{ij}^{\max}\frac{\gamma_{ij}^{f}(\gamma_{ij} - \gamma_{ij}^{\max})}{\gamma_{ij}(\gamma_{ij}^{f} - \gamma_{ij}^{\max})} \qquad \gamma_{ij}^{\max} < \gamma_{ij} \leq \gamma_{ij}^{f} \tag{10}$$

The final shear strain γ_{ij}^{f}, which corresponds to the end of the degradation phase, is related to the shear fracture energy.

The intralaminar failure models described above were implemented into the FE package ABAQUS/Explicit through a user-defined VUMAT subroutine. A characteristic length related to the element size and to the specific damage mode was introduced to reduce the mesh dependency associated to the smeared cracking approach.

3.2 Interlaminar failure

Delaminations between laminae with different fibre orientations were simulated by interface cohesive elements [13], defined by a traction-separation constitutive law consisting of an initial linear elastic stage until a stress-based damage initiation criterion is satisfied, followed by a linear softening phase that simulates the progressive decohesion of the interface with increasing damage. Complete fracture is assumed to occur when cohesive tractions vanish at the end of the degradation phase.

4 Impact modelling

A 3D FE model of the laminate sample was constructed in ABAQUS/Explicit using C3D8R solid elements for simulation of individual plies and zero-thickness COH3D8 cohesive elements for simulation of the interfaces between plies with different fibre orientations. The impactor and the supporting plate were modelled as rigid bodies using R3D4 rigid elements; the mass of 2.34 kg was imposed to the impactor through the definition of a mass element.

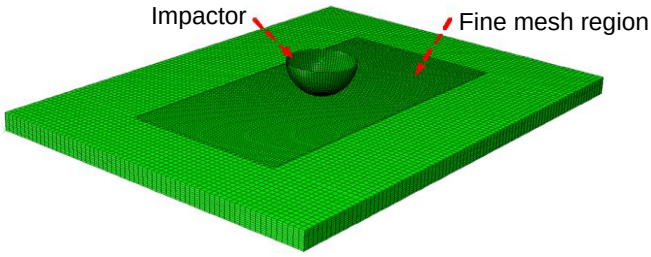

Figure 3. FE model for impact analyses

The elastic and fracture properties were obtained by a series of experimental tests. The main input properties used for the simulations were the following: E_{11}=122 GPa; E_{22}=E_{33}=6.20 GPa; ν_{12}= ν_{13}=0.35; ν_{23}=0.5; k_N=120 GPa/mm; k_S=k_T=43 GPa/mm; N=30 MPa; S=T=80 MPa; G_{IC}=520 J/m^2; G_{IIC}=G_{IIIC}=900 J/m^2; Due to the lack of experimental results for out-of-plane shear, the same curves for in-plane shear (Fig. 2) were used to model out-of-plane shear non-linearities.
Impacts of different energies were modelled by imposing the appropriate velocities at the instant of contact to the impactor. The interaction between the plate and the indentor was simulated by surface-to-surface contact pairs. No mass scaling was used in the analyses.
All analyses were performed on a distributed-memory cluster system of three Linux workstations (each with a quad-core Intel i7-860 processor and 8 GB RAM) interconnected with Gigabit Ethernet, using the MPI based parallel solver available in ABAQUS/Explicit.

5 Results and discussions

5.1 Structural response

Fig. 4 shows force vs. time and force vs. displacement plots as obtained by experimental tests and numerical simulations at various impact energy levels. It is seen that the computed results agree well with the experimental ones not only in duration of impact events but also in peak contact forces and absorbed energies (Fig. 5), which are calculated as the area under the force-displacement curve and represent the total energy dissipated in irreversible damage phenomena (intralaminar or interlaminar fracture, matrix plasticity).

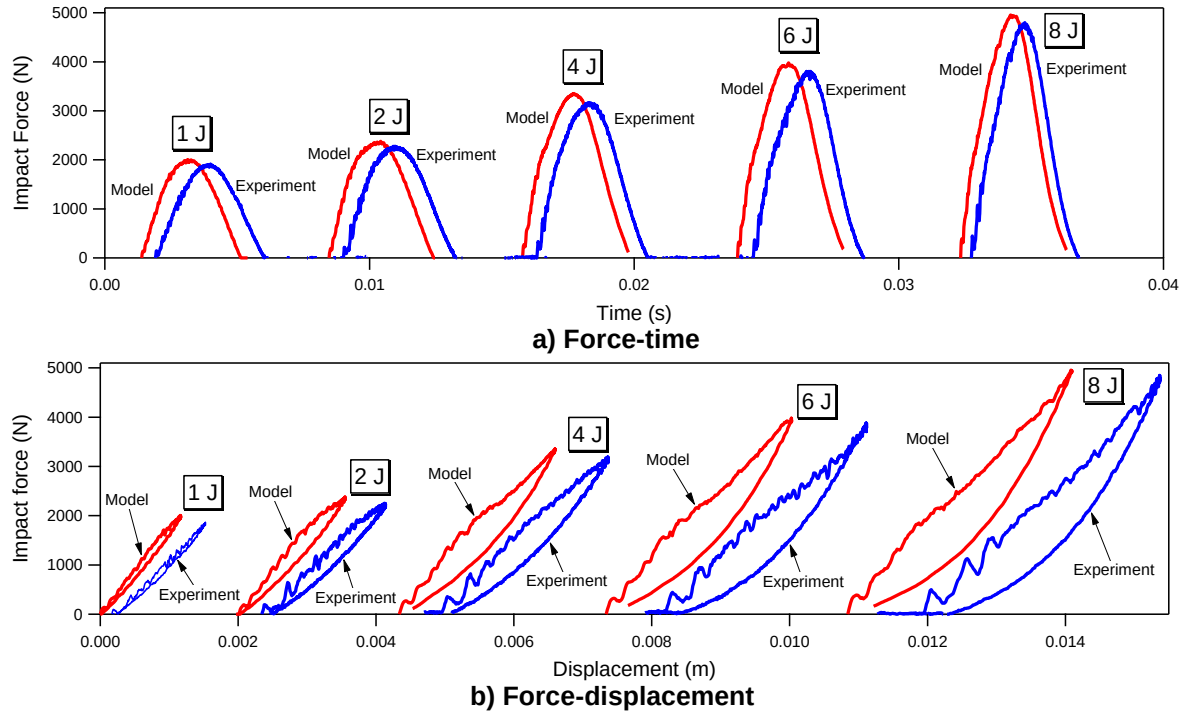

Figure 4. Comparison between experimental and numerical force-time (a) and force-displacement (b) curves

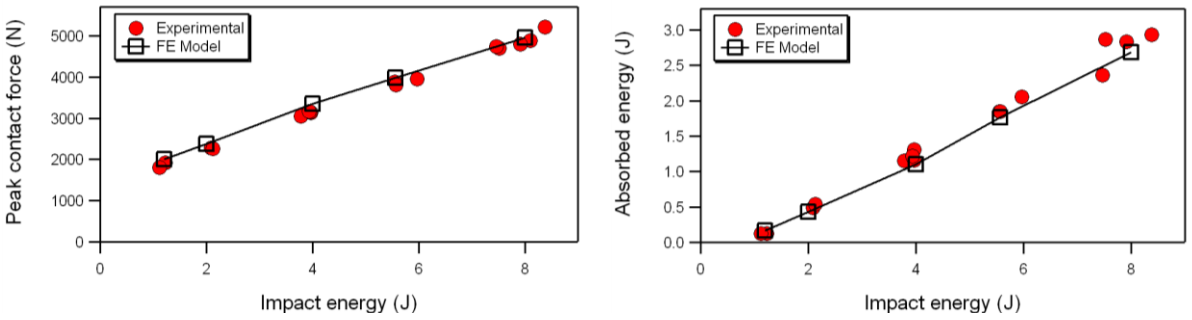

Figure 5. Comparison between experimental and predicted peak forces (left) and absorbed energies (right)

5.2 Internal damage

Fig. 6 reports experimental and computed projected damage areas at different impact energy levels. The comparison shows that the model is able to reproduce the geometry of the projected damage area and its principal orientation along the 0 ° direction. A detailed examination of the damage distribution through the thickness of the composite laminates shows that predicted shapes and depth locations of damage areas qualitatively agree with the experimental observations, as obtained by X-ray analyses. The model is not only capable of reproducing the two-lobe geometry and the main orientation of individual damage areas at selected depths (Fig. 6) but also able to predict with reasonable accuracy the damage sizes under various impact energies as shown in Fig. 7.

Further comparisons between numerical and experimental results for specific failure modes are illustrated in Fig. 8 for a 6 J impact. In agreement with experimental observations, the FE model predicts the growth of an extensive matrix crack in the bottom 0 ° layer, and also the initiation, at high impact energies, of fiber fracture in the impact region of the top 0 ° layer. The model is also able to correctly predict the development of delaminations at all interfaces, with a good qualitative accordance between simulation and X-ray observations in terms of shape and orientation of delaminated areas at individual interfaces. We may notice however that the size of the delamination at the +45/0 interface closer to the backface of the sample is

obviously under predicted in comparison with experimental evidence. Additional analyses are needed to clarify this aspect and to improve the prediction accuracy of the proposed damage model.

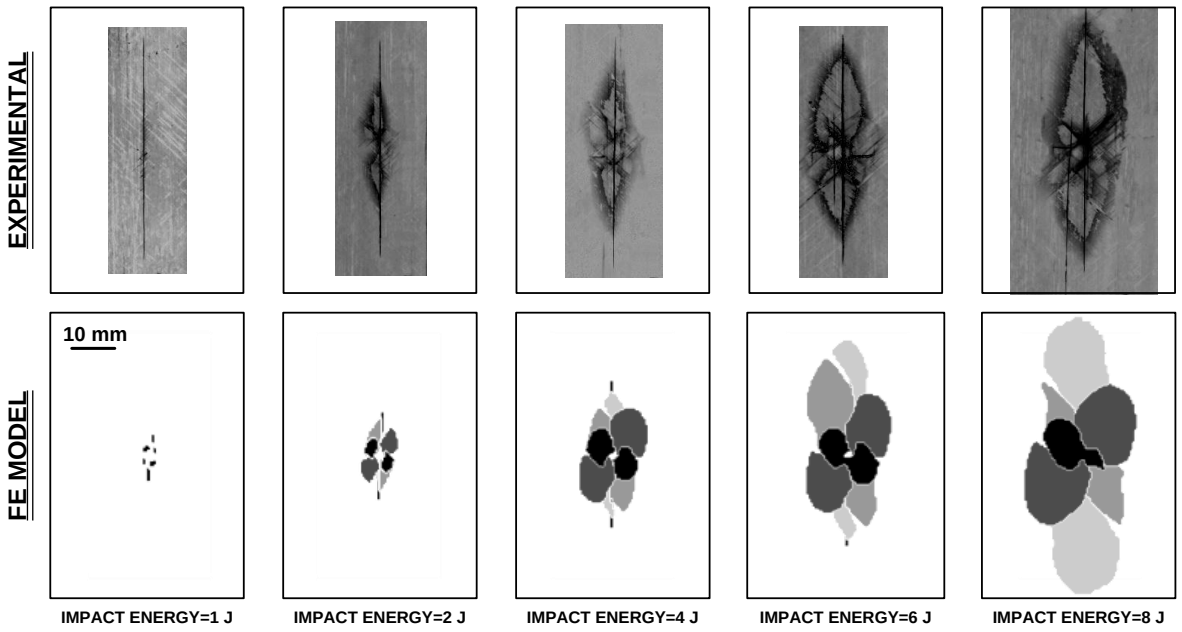

Figure 6. Comparison between projected damage areas as obtained by X-ray and predicted by FE model (different gray levels in predicted damage areas indicate different damage depths)

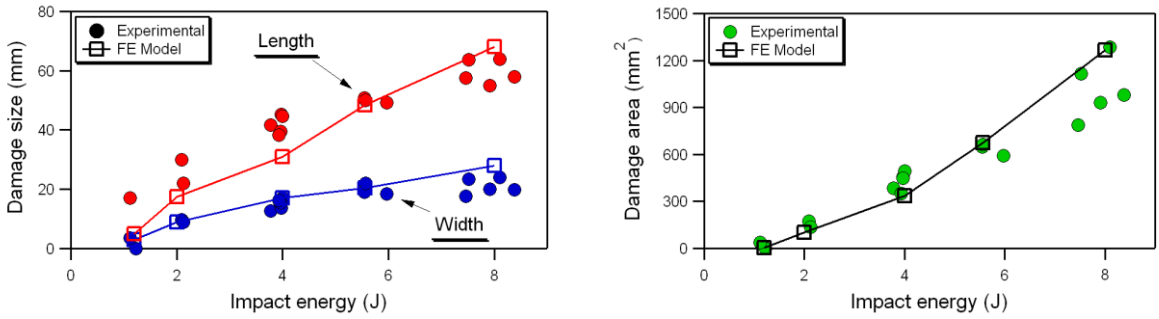

Figure 7. Comparison between experimental and predicted damage length/width (left) and damage areas (right)

6 Conclusions

In this study, a three-dimensional failure model for simulating various damage modes developing in composite laminates was implemented into the FE code ABAQUS/Explicit. The failure model was applied to simulate damage occurrence in laminated plates under transverse low-velocity impact. Comparisons between numerical predictions and experiment tests show reasonably good agreement in terms of structural response, energy absorption during impact and projected damage area.

Acknowledgements

This work has been supported by the EU funded FP7-ITN-Marie Curie project SYSWIND (Grant No. FP7-PEOPLE-ITN 238325).

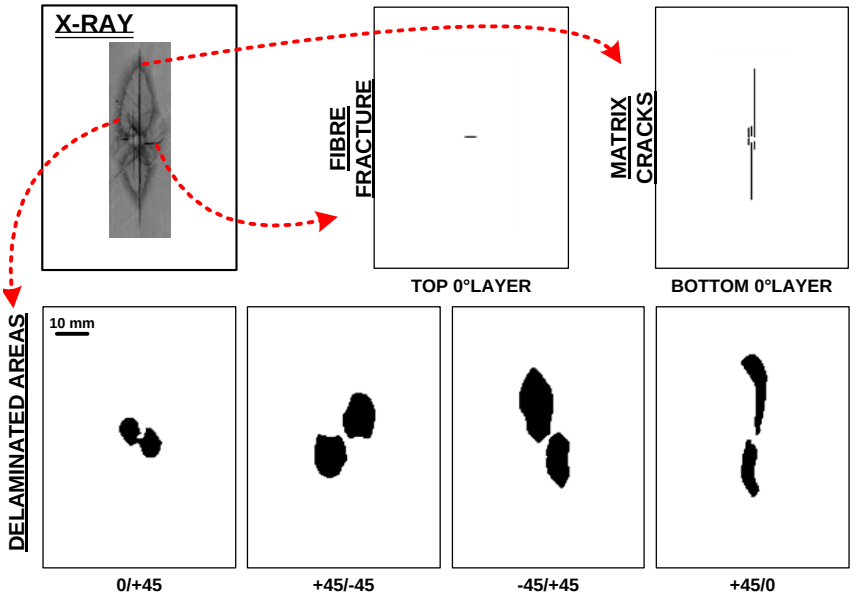

Figure 8. Different damage modes as predicted by the FE model for an impact energy of 6 J

References

[1] Abrate S. *Impact on composite structures.* Cambridge University Press, Cambridge (1998).

[2] Kachanov L.M. *Introduction to continuum damage mechanics*. Martinus Nijhoff Publsihers, Boston (1987).

[3] Lemaitre J., Chaboche J.L. *Mechanics of solid materials.* Cambridge University Press, Cambridge (1990).

[4] Iannucci L., Dechaene R., Willows M., Degrieck J. A failure model for the analysis of thin woven glass composite structures under impact loadings. *Computers and Structures*, **79(8)**, pp.785–799 (2001).

[5] Donadon M.V., Iannucci L., Falzon B.G., Hodgkinson J.M., de Almeida S.F.M. A progressive failure model for composite laminates subjected to low velocity impact damage. *Computers and Structures*, **86**, pp. 1232-1252 (2008).

[6] Pinho S.T., Davila C.G., Camanho P.P., Iannucci L., Robinson P. *Failure models and criteria for FRP under in-plane or three-dimensional stress states including shear non-linearity*, NASA/TM-2005-213530, HLRC (2005).

[7] Faggiani A., Falzon B.G. Predicting low-velocity impact damage on a stiffened composite panel. *Composites part A: Applied Science and Manufacturing*, **41**, pp. 737–749 (2010).

[8] Falzon B.G., Apruzzese P. Numerical analysis of intralaminar failure mechanisms in composite structures. Part I: FE implementation. *Composite Structures*, **93**, pp. 1039–1046 (2011).

[9] Falzon B.G., Apruzzese P. Numerical analysis of intralaminar failure mechanisms in composite structures. Part II: Applications. *Composite Structures*, **93**, pp. 1047–1053 (2011).

[10] Jones R.M. *Mechanics of composite materials*. Script Book Company, Washington (DC) (1975).

[11] Hashin Z. Failure criteria for unidirectional fiber composites. *Journal of Applied Mechanics*, **47(2)**, pp. 329–334 (1980).

[12] Schurmann H., Puck A. Failure analysis of FRP laminates by means of physically based phenomenological models. *Composites Science and Technology*, **62**, pp. 1633–1662 (2002).

[13] Aymerich F., Dore F., Priolo P. Prediction of impact-induced delamination in cross-ply composite laminates using cohesive interface elements. *Composites Science and Technology*, **68**, pp. 2383–2390 (2008).